

Chapter 6

Mixed Slip and Deceleration Control

6.1 Introduction

As has been discussed in the previous chapters (see in particular Chapter 3), in braking control systems, two output variables are usually considered for regulation purposes: wheel deceleration and wheel slip. Deceleration control and slip control are mostly viewed as alternative strategies; when deceleration and slip are both used, the typical approach is to regulate one variable and to keep the other variable within pre-defined thresholds.

In this chapter a braking control strategy that makes use of both wheel slip and wheel deceleration is presented and analysed. It is based on the idea of designing the braking controller as a classical feedback regulation loop, where the regulated variable is a convex combination of the wheel slip and the wheel deceleration. Accordingly, this control approach is concisely named *mixed slip-deceleration* (MSD) control. MSD is effective and flexible; it inherits all the attractive dynamical features of slip control, while strongly alleviating the detrimental effects of poor slip measurement. Moreover, by simply changing the design parameter that governs the relative weighting between slip and deceleration in forming the convex combination it is possible to emphasise different characteristics of the controller, according to different working conditions.

6.2 Mixed Slip-deceleration Control

The general structure of the proposed MSD control scheme is outlined in Figure 6.1. The transfer functions $G_\eta(s)$ and $G_\lambda(s)$ describing the linearised dynamics between wheel slip and braking torque and normalised wheel deceleration and braking torque, respectively, have been derived in (2.45) and (2.46) and are reported here for completeness

$$G_\eta(s) = \frac{\frac{r}{Jg} \left(s + \frac{\mu_1(\bar{\lambda})F_z}{m\bar{v}}(1 - \bar{\lambda}) \right)}{s + \frac{\mu_1(\bar{\lambda})F_z}{m\bar{v}} \left((1 - \bar{\lambda}) + \frac{mr^2}{J} \right)}, \quad (6.1)$$

$$G_\lambda(s) = \frac{\frac{r}{Jv}}{s + \frac{\mu_1(\bar{\lambda})F_z}{m\bar{v}} \left((1 - \bar{\lambda}) + \frac{mr^2}{J} \right)}. \quad (6.2)$$

By inspecting Figure 6.1, it is worth noticing that the noises on the deceleration and slip, d_η and d_λ respectively, are explicitly embedded in the control scheme. As in a classical control scheme, note that d_η and d_λ can represent both measurement noises and external disturbances acting on the system. In the rest of the chapter the notions of disturbance and measurement noise will be treated without explicit distinction. In practice, the emphasis here is on the measurement noise as this is the most critical aspect of slip control, since the accurate measurement of λ is well known to be rather challenging and critical (see Chapter 5).

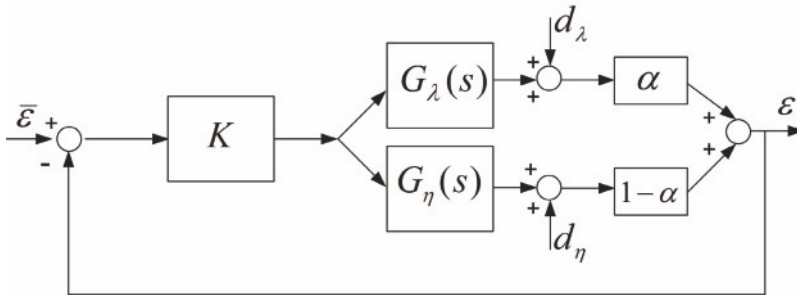


Figure 6.1 General scheme of the MSD controller

The basic idea of MSD control is to define an output controlled variable ϵ , which is the convex combination of the wheel normalised deceleration η and of the wheel slip λ , namely

$$\epsilon = \alpha\lambda + (1 - \alpha)\eta, \quad \alpha \in [0, 1], \quad (6.3)$$

and to regulate this variable to a set-point constant value $\bar{\epsilon}$ given by

$$\bar{\epsilon} = \alpha\bar{\lambda} + (1 - \alpha)\bar{\eta}. \quad (6.4)$$

Note that the set-point $\bar{\epsilon}$ itself can be interpreted as a convex combination of the set-points for wheel slip and wheel deceleration.

As was done in Chapter 3 for the case of wheel slip control, in order to focus on the heart of the control problem and to provide simple and insightful results, for analysis purposes a simple proportional controller is initially considered. Needless to say, the performance of the proportional controller

can be improved by employing a higher-order control architecture, but the basic results and conclusions remain unchanged, as will be shown later in this chapter.

It is interesting to notice that the MSD controller has the distinctive feature of embedding, as *extremal* cases, the slip controller ($\alpha = 1$) and the deceleration controller ($\alpha = 0$), which have been discussed in Sections 3.2 and 3.3. Now, the dynamic properties of the MSD controller will be studied.

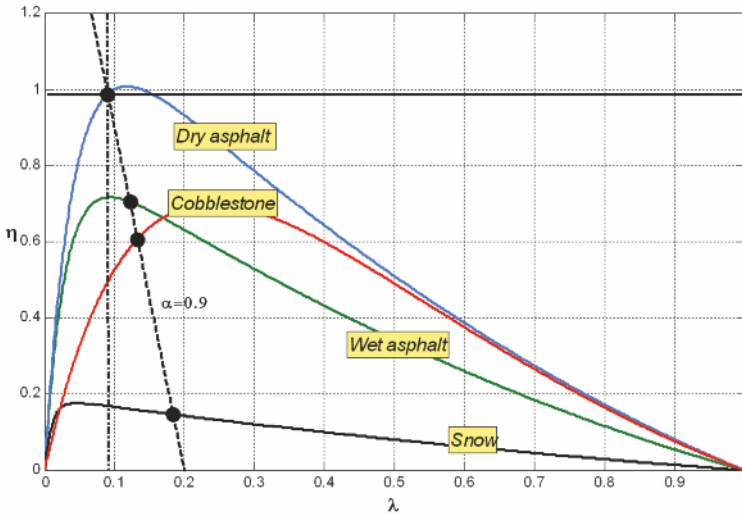


Figure 6.2 Equilibrium points for the MSD control in the (λ, η) plane with $\alpha = 0.9$ and $F_z = mg$

Figure 6.2 shows the equilibrium manifold in the (λ, η) plane given in Equation 2.34 for different road conditions, together with the corresponding graphical interpretation of the set-point $\bar{\varepsilon}$ given in (6.4) for $\alpha = 0.9$. The intersection points between the two curves represent the feasible equilibrium points for the closed-loop system.

By inspecting Figure 6.2 and recalling the expression of the equilibrium manifold for the wheel deceleration η as a function of λ in (2.34) and the expression of the set-point equation $\bar{\varepsilon}$ in (6.4), one may notice that the system equilibria are affected by the following four different factors.

1. The load transfer, represented by the term F_z/mg which is the ratio between the real vertical load F_z and its static value mg (see also Section 2.5). This factor, however, does not affect the qualitative properties of the equilibrium points. In fact, the the steady-state relationship between η and λ has the form

$$\eta(\lambda) = \frac{F_z}{mg}(1 - \lambda)\mu(\lambda).$$

Hence, the dynamic load transfer effect acts in the same way as a scaling factor in the tyre-road friction characteristic.

2. The tyre-road friction condition described by $\mu(\lambda)$, according to which the equilibrium point may vary (see Figure 6.2).
3. The set-point $\bar{\varepsilon}$. A change in the set-point corresponds to a rigid translation of the line $\bar{\varepsilon}(\eta, \lambda)$ (dashed line in Figure 6.2) which changes the equilibrium point and can affect its uniqueness.
4. The coefficient α , which determines the slope of the line $\bar{\varepsilon}(\eta, \lambda)$ in the (λ, η) plane (dashed line in Figure 6.2). This is the distinctive feature of the MSD control approach. In fact, for $\alpha = 1$ (vertical dash-dotted line in Figure 6.2) we have a genuine *slip control*. In this case, for any $\bar{\varepsilon} \in [0, 1]$ there always exists a unique equilibrium for all road conditions. On the other hand, for $\alpha = 0$ (horizontal solid line in Figure 6.2) we have a *deceleration control*; in this case there exist some values of the set-point for which two equilibria exist on some road conditions and none on other road conditions (see also Sections 3.2 and 3.3). For continuity, these two extremal conditions must be separated by a *threshold* (or lower bound) on α , located between 0 and 1, above which the equilibrium uniqueness is guaranteed. It will be shown that a good trade-off between slip and deceleration control is obtained for values of $\alpha \in [0.8, 1]$. Hence, the existence and uniqueness of the equilibrium points are deeply interlaced with the choice of this parameter, as will be further discussed in the following.

6.2.1 Analysis of the Open-loop Dynamics

From the dynamical viewpoint, the open-loop transfer function $G_\varepsilon(s)$ from δT_b to $\delta \varepsilon$ can be computed combining the transfer functions $G_\eta(s)$ and $G_\lambda(s)$ via the convex combination defined by (6.3).

Specifically, it has the form

$$\begin{aligned}
 G_\varepsilon(s) &= \frac{r}{J} \frac{\frac{1-\alpha}{g} \left[s + \frac{\mu_1(\bar{\lambda})F_z}{m\bar{v}} (1 - \bar{\lambda}) \right] + \frac{\alpha}{\bar{v}}}{s + \frac{\mu_1(\bar{\lambda})F_z}{m\bar{v}} \left((1 - \bar{\lambda}) + \frac{mJ^2}{J} \right)} \\
 &= \frac{(1 - \alpha)r}{Jg} \frac{s + \left(\frac{\mu_1(\bar{\lambda})F_z}{m\bar{v}} (1 - \bar{\lambda}) + \frac{g}{\bar{v}} \frac{\alpha}{1 - \alpha} \right)}{s + \frac{\mu_1(\bar{\lambda})F_z}{m\bar{v}} \left((1 - \bar{\lambda}) + \frac{mJ^2}{J} \right)}.
 \end{aligned} \tag{6.5}$$

By analysing (6.5), the stability properties of the linearised system having the braking torque as input and ε as output can be easily studied.

Specifically, note that the linearised single-corner model with transfer function $G_\varepsilon(s)$ is asymptotically stable if and only if

$$\frac{\mu_1(\bar{\lambda})F_z}{m\bar{v}} \left((1 - \bar{\lambda}) + \frac{mr^2}{J} \right) > 0,$$

which, as both summands in the brackets are positive, reduces to $\mu_1(\bar{\lambda}) > 0$. Hence, $G_\varepsilon(s)$ has a real positive pole if the equilibrium wheel slip value $\bar{\lambda}$ occurs beyond the peak of the curve $\mu(\lambda)$, which is the same result found in Chapter 3 for $G_\lambda(s)$ and $G_\eta(s)$.

Further, it is interesting to investigate the position of the (real) zero of $G_\varepsilon(s)$ as a function of the parameter α . Specifically, the zero of $G_\varepsilon(s)$ is negative if and only if

$$\frac{\mu_1(\bar{\lambda})F_z}{m\bar{v}}(1 - \bar{\lambda}) + \frac{g}{\bar{v}} \frac{\alpha}{1 - \alpha} > 0.$$

Thus, if $\mu_1(\bar{\lambda}) > 0$ the zero is negative for all possible values of $\alpha \in [0, 1)$, whereas, if $\mu_1(\bar{\lambda}) < 0$, to have a negative zero one needs

$$\frac{\alpha}{(1 - \alpha)} > -\frac{\mu_1(\bar{\lambda})F_z}{mg} (1 - \bar{\lambda}).$$

Thus, it is always possible to find a value of α , say $\bar{\alpha}$, such that, for $\bar{\alpha} < \alpha < 1$, the zero of $G_\varepsilon(s)$ is negative (in practice, $\bar{\alpha} \cong 0.3$ is enough to guarantee this in every road condition and for every value of $\bar{\lambda}$).

6.2.2 Closed-loop Stability for MSD Control

Consider now the MSD closed-loop system shown in Figure 6.1. In this case, the characteristic polynomial $\chi_\varepsilon(s, \alpha)$ is given by

$$\begin{aligned} \chi_\varepsilon(s, \alpha) = s & \left[1 + \frac{Kr}{Jg}(1 - \alpha) \right] \\ & + \frac{1}{\bar{v}} \left[\frac{\mu_1(\bar{\lambda})F_z}{m} \left((1 - \bar{\lambda}) \left(1 + \frac{Kr}{Jg}(1 - \alpha) \right) + \frac{mr^2}{J} \right) + \alpha \frac{Kr}{J} \right]. \end{aligned}$$

Accordingly, the following stability condition can be determined (note that, as was the case also for slip and deceleration control, see Sections 3.2 and 3.3), it does not depend on \bar{v})

$$\frac{\mu_1(\bar{\lambda})F_z}{m} \left((1 - \bar{\lambda}) \left(1 + K \frac{r}{Jg}(1 - \alpha) \right) + \frac{mr^2}{J} \right) + K\alpha \frac{r}{J} > 0.$$

Note that for a fixed value of $\alpha \in (0, 1)$ and for large values of K this condition can be simplified as follows:

$$(1 - \alpha) \frac{\mu_1(\bar{\lambda}) F_z}{mg} (1 - \bar{\lambda}) + \alpha > 0.$$

From the above condition it can be easily shown that if $\mu_1(\bar{\lambda}) > 0$ the condition is fulfilled for all feasible values of α , while to ensure closed-loop stability for wheel slip values beyond the peak of the friction curve (*i.e.*, when $\mu_1(\bar{\lambda}) < 0$), one needs to choose the value of the parameter α such that $\alpha_{\text{Min}} < \alpha \leq 1$, where

$$\alpha_{\text{Min}} = \max_{\bar{\lambda}, \vartheta_r} \left\{ \frac{\mu_1(\bar{\lambda}; \vartheta_r) (\bar{\lambda} - 1) \frac{F_z}{mg}}{1 + \mu_1(\bar{\lambda}; \vartheta_r) (\bar{\lambda} - 1) \frac{F_z}{mg}} \right\}. \quad (6.6)$$

If α is fixed based on (6.6) it is always possible to find a value \bar{K} such that, for $K > \bar{K}$, the closed-loop system is asymptotically stable in every working condition (namely for every value of $\bar{\lambda}$ and for every road condition, represented in (6.6) by the parameters ϑ_r which define the different tyre–road friction conditions in the model given in (2.13)).

Given the previous stability results for slip control and deceleration control, condition (6.6) was somehow to be expected; we have seen in Chapter 3 that for $\alpha = 1$ (wheel slip control) stability can be always guaranteed, whereas for $\alpha = 0$ (wheel deceleration control) it is impossible to find a unique stabilising proportional controller. For continuity, these two extremal conditions must be separated by a *threshold* on α , located between 0 and 1. Expression (6.6) is interesting since it provides, in a simple closed-form, the analytic expression of this threshold α_{Min} .

Note that the lower bound (6.6) is computed as the worst case with respect to both the equilibrium point $\bar{\lambda}$ and the road conditions modelled *via* ϑ_r . In Figure 6.3 the expression

$$\frac{\mu_1(\bar{\lambda}; \vartheta_r) (\bar{\lambda} - 1) \frac{F_z}{mg}}{1 + \mu_1(\bar{\lambda}; \vartheta_r) (\bar{\lambda} - 1) \frac{F_z}{mg}} \quad (6.7)$$

is displayed, as a function of $\bar{\lambda}$, for different road conditions (it is clipped at zero when $\mu_1(\bar{\lambda}) > 0$). Figure 6.3 shows that the most demanding conditions as far as the lower bound on α is concerned are given by

- values of $\bar{\lambda}$ beyond the peak of the friction curve; and
- high-grip road conditions.

From Figure 6.3 an estimation of α_{Min} can be derived: $\alpha_{\text{Min}} \cong 0.3$. Note that this value has a simple and intuitive interpretation, similar to that given in Section 3.2 for the minimum controller gain needed to stabilise the closed-loop system with a proportional wheel slip controller.

To see this with reference to the (λ, η) plane, consider that the set-point line $\varepsilon = \bar{\varepsilon}$ in (6.4) can be expressed as a function of η as

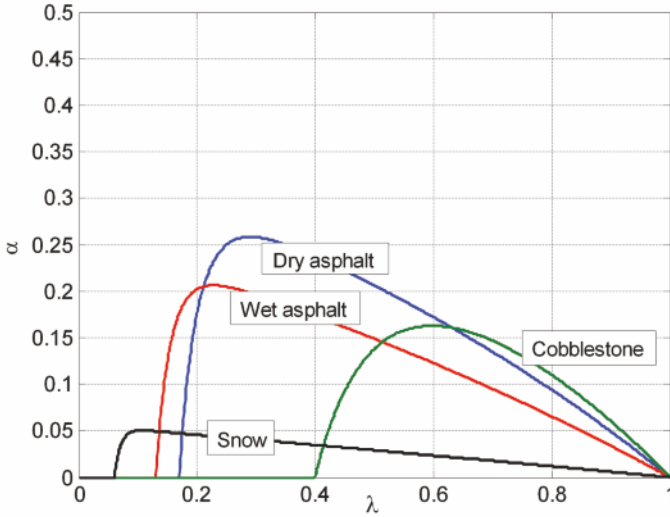


Figure 6.3 Plot of the lower bound on the parameter α in (6.7) as a function of λ , for different road conditions and $F_z = mg$

$$\bar{\eta} = -\frac{\alpha}{1-\alpha}\bar{\lambda} + \frac{1}{1-\alpha}\bar{\varepsilon}. \tag{6.8}$$

Thus, the effect of a proportional controller with gain K can be expressed as a function of η as

$$\bar{\eta} = -K \left[\frac{\alpha}{1-\alpha}\bar{\lambda} + \frac{1}{1-\alpha}\bar{\varepsilon} \right]. \tag{6.9}$$

Hence, the lower bound α_{Min} is the minimum value of α that guarantees that the set-point for the MSD control in (6.8) (see the dashed line in Figure 6.2) has an angular coefficient $-\frac{\alpha}{1-\alpha}$ large enough to ensure that when a proportional controller is used, there exists a minimum value \bar{K} of the gain so that for all $K > \bar{K}$ in the closed-loop system there exists a single equilibrium point. Such an equilibrium is given by the intersection between the equilibrium manifold in the (λ, η) plane and the line in (6.9) and it is locally asymptotically stable for all choices of $\bar{\lambda}$ and for all road conditions.

At the end of this analysis, one can concisely conclude that if $\alpha_{\text{Min}} < \alpha < 1$, MSD control essentially shares the same appealing features as slip control: unique equilibrium, fixed set-point, fixed controller structure. In practice, in order to achieve almost-optimal braking performance with fixed values of α and $\bar{\varepsilon}$, α must be chosen close to 1, as will be clear once the disturbance rejection properties of the MSD controller will be analysed.

A non-negligible advantage of MSD control over slip control is the left half plane zero in the open-loop transfer function (6.5). Note that, more precisely, the advantage of this zero is easy to understand when a linearisation

of the plant dynamics around a locally asymptotically stable equilibrium point is considered. On the other hand, when the considered equilibrium point is unstable, the advantage of this left half plane zero remains, but its explanation is less intuitive.

The major advantage of MSD control, however, is its reduced sensitivity (with respect to slip control) to poor slip measurement. This is a key issue and will be extensively discussed in the following section. It will be shown that while preserving all the appealing features of slip control, MSD control is characterised by superior noise attenuation properties.

6.3 Disturbance Analysis of Slip Control and MSD Control

Consider the general MSD control structure in the block diagram of Figure 6.1. It is easy to see that – in the closed-loop system – the disturbance $d_\varepsilon(\alpha)$ affecting the controlled variable ε is related to the slip and deceleration disturbances d_λ and d_η as follows:

$$D_\varepsilon(s, \alpha) = [\alpha D_\lambda(s) + (1 - \alpha) D_\eta(s)] S_\varepsilon(s, \alpha),$$

where $D_\varepsilon(s; \alpha)$, $D_\lambda(s)$ and $D_\eta(s)$ are the Laplace-transforms of the signals d_ε , d_λ and d_η , respectively, and $S_\varepsilon(s; \alpha)$ is the closed-loop sensitivity function, given by

$$S_\varepsilon(s; \alpha) = \frac{s + \frac{\mu_1(\bar{\lambda})F_z}{m\bar{v}} \left((1 - \bar{\lambda}) + \frac{mr^2}{J} \right)}{s \left[1 + K \frac{r}{Jg} (1 - \alpha) \right] + \frac{1}{\bar{v}} \left[\frac{\mu_1(\bar{\lambda})F_z}{m} \left((1 - \bar{\lambda}) \left(1 + \frac{Kr}{Jg} (1 - \alpha) \right) + \frac{mr^2}{J} \right) + K\alpha \frac{r}{J} \right]}. \quad (6.10)$$

We now want to investigate the dependency of the closed-loop disturbance $d_\varepsilon(\alpha)$ on the weighting parameter α . More specifically, we want to analyse the following function:

$$\gamma(\alpha) = \frac{\text{Var}[d_\varepsilon(\alpha)]}{\text{Var}[d_\varepsilon(1)]}, \quad (6.11)$$

where $d_\varepsilon(1)$ represents the disturbance in the case of wheel slip control, *i.e.*, for $\alpha = 1$. Thus, $\gamma(\alpha)$ is the ratio between the variance of the disturbance acting on the output variable in MSD control and the that in wheel slip control (note in fact that $\gamma(1) = 1$). In order to develop this analysis, three simple preliminary assumptions are made.

1. It is assumed that the measured output variables λ and η are affected by zero-mean, uncorrelated, band-limited white noises d_λ and d_η in the

frequency range $[0, \Omega_N]$, Ω_N being the Nyquist frequency of the sampled signals: $d_\lambda \approx WN(0, \sigma_\lambda^2)$, $d_\eta \approx WN(0, \sigma_\eta^2)$. Notice that, in practice, all the measured signals are digitally sampled at the frequency of $2\Omega_N$; in order to keep the continuous-time notation used throughout the chapter, a band-limited white noise assumption must be made.

2. It is also assumed that $\sigma_\lambda^2 \gg \sigma_\eta^2$. This is motivated by the fact that the noise on the wheel deceleration only comes from the wheel encoder signal processing and the differentiation, while that on the wheel slip is also affected by the vehicle speed estimation error (see Appendix B and Chapter 5).
3. Large values of the feedback gain K are considered, the parameter α is assumed to be close to 1 ($0.8 \leq \alpha \leq 0.95$), and the slip values are assumed to be non-negligible (*i.e.*, $\bar{\lambda} > 0.07$).

First, it is easy to see that $\gamma(\alpha)$ can be re-written as the product of two factors as

$$\gamma(\alpha) = \frac{\text{Var}[d_\varepsilon(\alpha)]}{\text{Var}[d_\varepsilon(1)]} = \Psi(\alpha)\Phi(\alpha),$$

where

$$\Psi(\alpha) = \frac{\alpha^2\sigma_\lambda^2 + (1-\alpha)^2\sigma_\eta^2}{\sigma_\lambda^2}$$

and

$$\Phi(\alpha) = \frac{\int_{\omega=0}^{\Omega_N} |S_\varepsilon(j\omega; \alpha)| d\omega}{\int_{\omega=0}^{\Omega_N} |S_\varepsilon(j\omega; 1)| d\omega}.$$

The analysis of the first factor $\Psi(\alpha)$ is very simple. As we assumed that $0.8 \leq \alpha \leq 0.95$ and that $\sigma_\lambda^2 \gg \sigma_\eta^2$, $\Psi(\alpha)$ can be approximated as follows:

$$\Psi(\alpha) \cong \alpha^2.$$

Clearly, this factor has little influence on the noise attenuation properties (a slightly better attenuation in the case of MSD control is provided with respect to wheel slip control).

The analysis of the factor $\Phi(\alpha)$ is far more complicated. This analysis can be carried out by inspecting the main features of the magnitude of the frequency response of the sensitivity function (6.10), which is a first-order transfer function, characterised by a pole and a zero. For the analysis of $\Phi(\alpha)$, the behaviour of $S_\varepsilon(s; \alpha)$ can be condensed into four main features: the high-frequency gain, the low-frequency (DC) gain, the angular frequency position of the zero and the angular frequency position of the pole. A simple qualitative analysis and discussion of these four features is now provided.

High-frequency Gain: HF(α)

From Equation 6.10, HF(α) can be computed as

$$\text{HF}(\alpha) = \frac{1}{1 + K \frac{r}{Jg}(1 - \alpha)}. \quad (6.12)$$

This term shows that MSD control can provide a large attenuation benefit at high frequencies. As a matter of fact the HF gain for slip control HF(1) = 1, whereas, for large values of K , HF(α) \ll 1.

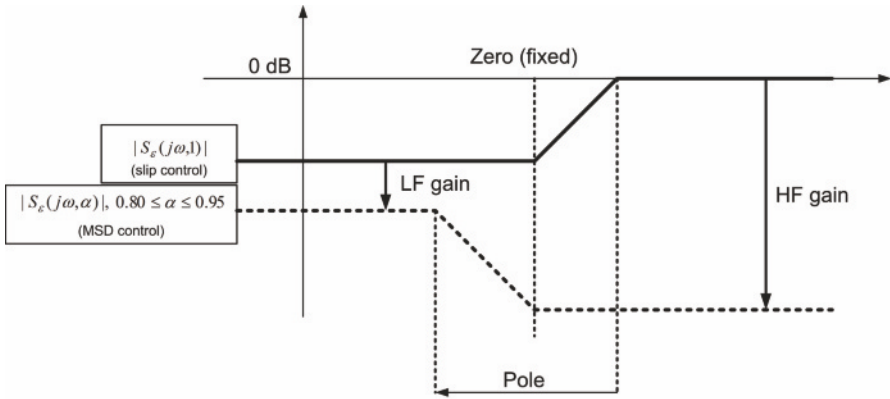


Figure 6.4 Sensitivity function features, when $\alpha = 1$ and $0.8 \leq \alpha \leq 0.95$

Low-frequency gain: LF(α)

From Equation 6.10, LF(α) can be computed as

$$\text{LF}(\alpha) = \frac{\frac{\mu_1(\bar{\lambda})F_z}{m} \left((1 - \bar{\lambda}) + \frac{mr^2}{J} \right)}{\frac{\mu_1(\bar{\lambda})F_z}{m} \left((1 - \bar{\lambda}) \left(1 + K \frac{r}{J}(1 - \alpha) \right) + \frac{mr^2}{J} \right) + K\alpha \frac{r}{J}}. \quad (6.13)$$

The analysis of Equation 6.13 is less trivial than that of Equation 6.12. For the analysis of the attenuation benefits achievable with MSD control it is useful to analyse the ratio LF(α)/LF(1)

$$\frac{\text{LF}(\alpha)}{\text{LF}(1)} = \frac{\left[\frac{\mu_1(\bar{\lambda})F_z}{m} \left((1 - \bar{\lambda}) + \frac{mr^2}{J} \right) \right] + \left[K \frac{r}{J} \right]}{\left[\frac{\mu_1(\bar{\lambda})F_z}{m} \left((1 - \bar{\lambda}) + \frac{mr^2}{J} \right) \right] + \left[K\alpha \frac{r}{J} \right] + \left[\frac{\mu_1(\bar{\lambda})F_z}{m} (1 - \bar{\lambda})(1 - \alpha) K \frac{r}{J} \right]}. \quad (6.14)$$

Note that the dominant term both in the numerator and in the denominator of (6.14) is

$$\frac{K \frac{r}{J}}{K \alpha \frac{r}{J}} = \frac{1}{\alpha} \cong 1.$$

The LF gain ratio (6.14) henceforth is approximately equal to 1. More specifically, when $\mu_1(\bar{\lambda}) > 0$, note that all the terms at the denominator of Equation 6.14 are positive; hence, in this case, $\text{LF}(\alpha)/\text{LF}(1)$ can be significantly lower than 1. When $\mu_1(\bar{\lambda}) < 0$, notice that the third term in the denominator is small, since, despite the presence of K , the factors $(1 - \bar{\lambda})$, $(1 - \alpha)$ and $|\mu_1(\bar{\lambda})|$ are all very small; henceforth, $\text{LF}(\alpha)/\text{LF}(1) \cong 1$.

We can conclude that at low frequencies the MSD control and the slip control provide almost the same attenuation (or MSD control can provide a small attenuation benefit).

Frequency-domain Position of the Zero: $Z(\alpha)$

The angular frequency of the zero does not depend on the parameter α ; it is given by

$$Z(\alpha) = Z(1) = \left| \frac{\mu_1(\bar{\lambda})F_z}{m} \left((1 - \bar{\lambda}) + \frac{mr^2}{J} \right) \right|.$$

Frequency-domain Position of the Pole: $P(\alpha)$

The angular frequency of the pole is given by

$$P(\alpha) = \left| \frac{\frac{1}{v} \left[\frac{\mu_1(\bar{\lambda})F_z}{m} \left((1 - \bar{\lambda}) \left(1 + K \frac{r}{J} (1 - \alpha) \right) + \frac{mr^2}{J} \right) + K \alpha \frac{r}{J} \right]}{\left[1 + K \frac{r}{Jg} (1 - \alpha) \right]} \right|. \quad (6.15)$$

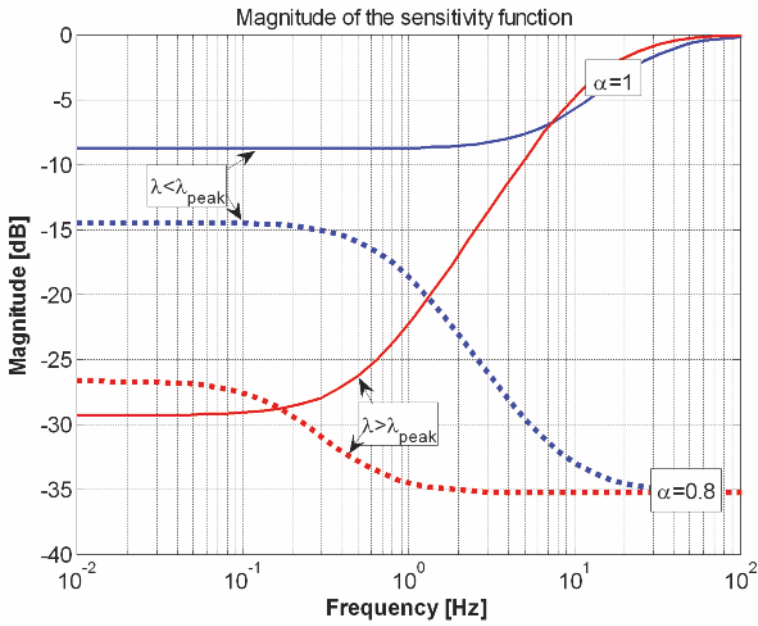
It is interesting to analyse the relative position of the pole, for $0.8 \leq \alpha \leq 0.95$, and for $\alpha = 1$, namely

$$\frac{P(\alpha)}{P(1)} = \left| \frac{\left[\frac{\mu_1(\bar{\lambda})F_z}{m} \left((1 - \bar{\lambda}) \left(1 + K \frac{r}{J} (1 - \alpha) \right) + \frac{mr^2}{J} \right) + K \alpha \frac{r}{J} \right]}{\left[\frac{\mu_1(\bar{\lambda})F_z}{m} \left((1 - \bar{\lambda}) + \frac{mr^2}{J} \right) + K \frac{r}{J} \right] \left[1 + K \frac{r}{Jg} (1 - \alpha) \right]} \right|. \quad (6.16)$$

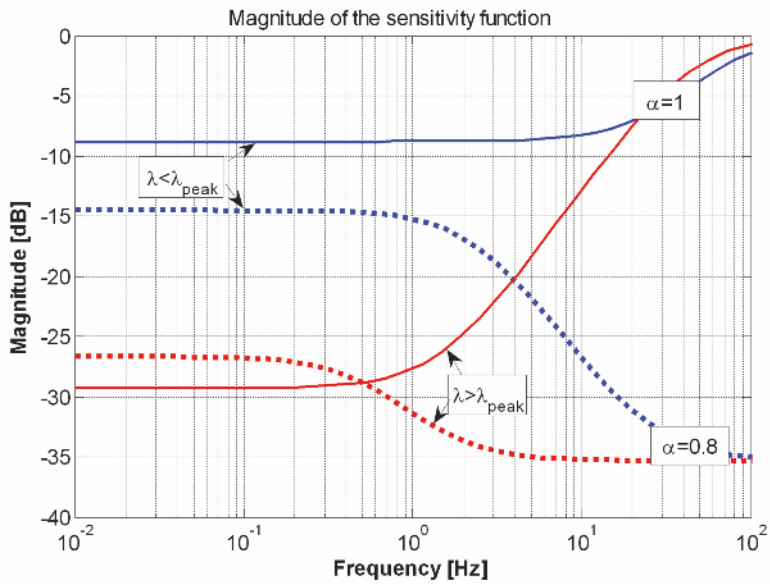
The analysis of Equation 6.16 clearly shows that the pole angular frequency decreases when α decreases, since the ratio $P(\alpha)/P(1)$ is dominated by the factor

$$1 + K \frac{r}{Jg} (1 - \alpha)$$

at the denominator.



(a)



(b)

Figure 6.5 Bode plot of the frequency response associated with the sensitivity function: behaviour for $v = 30$ m/s (a) and for $v = 10$ m/s (b)

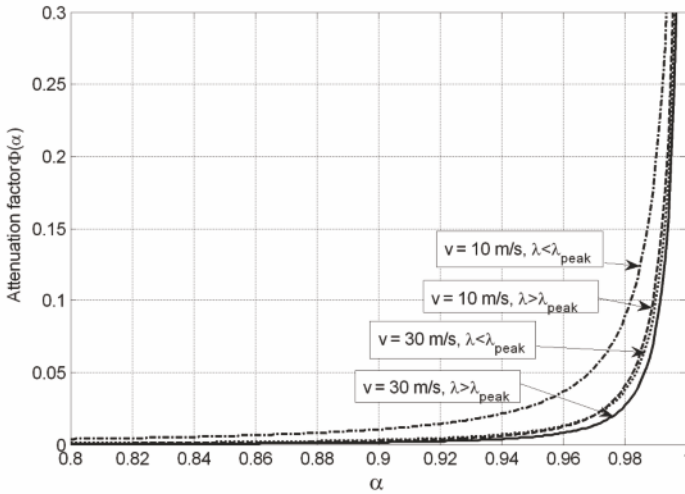


Figure 6.6 Plot of $\Phi(\alpha)$ in different working conditions

The results of the above analysis of $|S_\varepsilon(s; \alpha)|$ and $|S_\varepsilon(s; 1)|$ can be summarised as in Figure 6.4:

- The LF gain is slightly sensitive to α ; moving from $\alpha = 1$ to $0.8 \leq \alpha \leq 0.95$, it remains almost unchanged, or it can slightly decrease.
- The HF gain strongly decreases when $0.8 \leq \alpha \leq 0.95$.
- The angular frequency of the zero is unchanged, whereas that of the pole decreases when $0.8 \leq \alpha \leq 0.95$.

These approximate results are confirmed by Figures 6.5(a) and 6.5(b), where the magnitude Bode plots of the frequency response associated with the sensitivity function for $\alpha = 1$ and $\alpha = 0.8$ are displayed for different conditions (two different forward speed values and two different values of $\bar{\lambda}$). The analysis of the magnitude Bode plots of the frequency response associated with $S_\varepsilon(s; \alpha)$ clearly shows that the factor $\Phi(\alpha)$ rapidly becomes much lower than 1 when $\alpha < 1$.

In order to have a more immediate feeling on the attenuation level, in Figure 6.6 the behaviour of $\Phi(\alpha)$ is displayed in the range $\alpha \in [0.8, 1]$, for different conditions (two different forward speed values, and two different values of $\bar{\lambda}$). Interestingly enough, it can be observed that:

- As α moves from $\alpha = 1$ to $\alpha < 1$, $\Phi(\alpha)$ decreases very rapidly (*e.g.*, in every condition, if $\alpha = 0.95$, the value of $\Phi(\alpha)$ is lower than 0.05). This means that a slight use of the wheel deceleration in the feedback controlled variable is enough to obtain large noise attenuation benefits.
- The spread of $\Phi(\alpha)$ is comparatively small. Thus, the attenuation effect is large in every working condition.

This analysis has shown that MSD control can provide large benefits in terms of noise attenuation with respect to slip control. This advantage has been assessed by means of a quantitative analysis.

6.4 Steady-state Slip Values in MSD Control

Before moving on to assess the MSD performance *via* simulation results, it is worth analysing the steady-state behaviour of the wheel slip when the vehicle is controlled *via* MSD control.

To perform the analysis, recall first that the the equilibrium manifold in the (λ, η) domain is given by

$$\eta(\lambda) = N(1 - \lambda)\mu(\lambda), \quad (6.17)$$

where $N = F_z/mg$, see also (2.53), is the ratio between the actual and the static vertical load. Thus, when MSD control is applied to the single-corner model, the dependence of the equilibrium point on the load transfer N makes the steady-state value of the wheel slip $\bar{\lambda}$ change according to the value of N itself. In fact, by imposing a set-point value $\bar{\varepsilon}$ one has to satisfy the relationship (6.4), *i.e.*,

$$\bar{\varepsilon} = \alpha\bar{\lambda} + (1 - \alpha)\bar{\eta}.$$

Thus, if N increases, the set-point value $\bar{\eta}$ increases in view of (6.17) and thus the steady-state wheel slip $\bar{\lambda}$ decreases to satisfy the set-point expression (6.4).

To see this, consider Figure 6.7, which shows the time histories of the closed-loop front and rear wheel slip in a hard braking manoeuvre on dry asphalt in four different cases: the front wheel slip obtained when only the front wheels are controlled (dashed line), the rear wheel slip obtained when only the rear wheels are controlled (dash-dotted line) and the front (dotted line) and rear (solid line) wheel slip obtained when all four wheels are controlled via MSD control with equal values for $\bar{\varepsilon}$ and α .

As can be seen, when only the front or the rear wheels are controlled with the same $\bar{\varepsilon}$ and α , the steady-state wheel slip is different and, consistently with what has been previously noticed, lower at the front wheels (where N is larger) and higher at the rear wheels (where N is smaller).

However, in a full vehicle setting, that is when the same MSD controller (*i.e.*, with a common set-point value $\bar{\varepsilon}$ and an equal value for α) is used to regulate each of the four wheels, the steady-state value of the wheel slip goes back to being the same at all wheels.

To see this, consider for simplicity the double-corner model, where the longitudinal chassis dynamics is given by (see also Section 2.4)

$$\dot{v} = -\frac{1}{m}(F_{zf}\mu(\lambda_f) + F_{zr}\mu(\lambda_r)), \quad (6.18)$$

where F_{zf} and F_{zr} are the vertical forces at the front and rear wheel and λ_f and λ_r are the front and rear wheel slip, respectively.

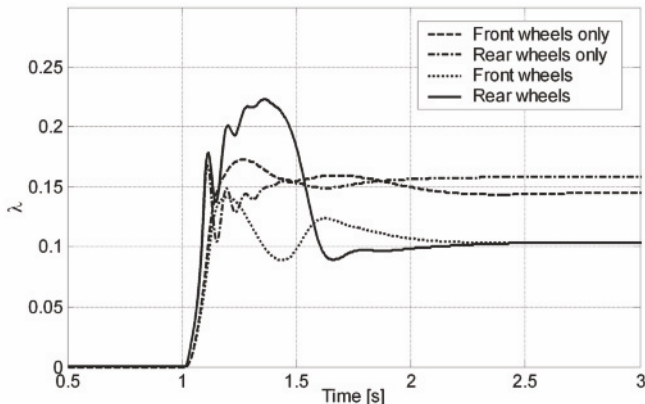


Figure 6.7 Time histories of the wheel slip during a hard braking manoeuvre on dry asphalt: front wheel slip when only the front wheels are controlled (*dashed line*), rear wheel slip when only the rear wheels are controlled (*dash-dotted line*) and front (*dotted line*) and rear (*solid line*) wheel slip when all four wheels are controlled

Recalling now the analysis in Section 2.5.1 one has that, letting $\dot{\lambda}_i = 0$, $i = \{f, r\}$, the expression linking the wheel acceleration $\dot{\omega}_i$ and the chassis acceleration \dot{v} has the form

$$\dot{\omega}_i = \frac{1 - \lambda_i}{r_i} \dot{v}. \quad (6.19)$$

Accordingly, recalling that $\eta_i = -\dot{\omega}_i r_i / g$, and substituting into this relationship the expression for \dot{v} in (6.18) one has

$$\bar{\eta}_i = \frac{(F_{zf}\mu(\bar{\lambda}_f) + F_{zr}\mu(\bar{\lambda}_r))}{mg} (1 - \bar{\lambda}_i) = \zeta(\bar{\lambda}_f, \bar{\lambda}_r) (1 - \bar{\lambda}_i), \quad (6.20)$$

where the term $\zeta(\bar{\lambda}_f, \bar{\lambda}_r)$ is the same for the front and for the rear wheel.

Further, imposing the same MSD control set-point for the controlled variable, *i.e.*, $\bar{\varepsilon}_i = \bar{\varepsilon}$, $i = \{f, r\}$, the expression for the equilibrium values of $\bar{\eta}_i$ becomes

$$\bar{\eta}_i = \frac{1}{1 - \alpha} \bar{\varepsilon} - \frac{\alpha}{1 - \alpha} \bar{\lambda}_i. \quad (6.21)$$

Combining Equation 6.21 with Equation 6.20 and solving for $\bar{\lambda}_i$, one obtains

$$\bar{\lambda}_i = \frac{\zeta(\bar{\lambda}_f, \bar{\lambda}_r) - \frac{1}{1-\alpha}\bar{\epsilon}}{\zeta(\bar{\lambda}_f, \bar{\lambda}_r) - \frac{\alpha}{1-\alpha}}, \quad (6.22)$$

which shows that, at steady-state, the wheel slip value will be the same at the front and rear wheels, *i.e.*, $\bar{\lambda}_i = \bar{\lambda}$.

This allows us to re-write the term $\zeta(\bar{\lambda}_f, \bar{\lambda}_r)$ as

$$\zeta(\bar{\lambda}_f, \bar{\lambda}_r) = \mu(\bar{\lambda}) \left[\frac{(F_{zf} + F_{zr})}{mg} \right] = \mu(\bar{\lambda}), \quad (6.23)$$

where the last equality comes from the fact that $(F_{zf} + F_{zr})$ equals the overall vertical load, independently of its distribution between front and rear wheels.

Inspecting Figure 6.7 again, note that when both the front and rear controllers are employed, the steady-state wheel slip values are the same at all wheels, coherently with the performed analysis.

6.5 Numerical Analysis

The MSD control approach has been presented in the previous sections in a simplified setting: only the single-corner dynamics have been modelled and a simple proportional controller has been used. This simplified setting is particularly useful to focus on the heart of the control problem and to gain a deep insight in the algorithm behaviour.

However, the theoretical analysis developed in this simple setting must be corroborated by simulation results obtained on a full-vehicle simulator.

To implement the control algorithms in a fully-realistic setting, the simulation environment must also include the description of the EMB actuator dynamics given in (1.4). Finally, the simulations are performed replacing the proportional controllers with dynamic controller structures. More specifically:

- The wheel slip controller $R_\lambda(s)$ is implemented with the PID control architecture presented in Section 3.4, which has been tuned to work satisfactorily in every working condition (for different slip set-points, different road surfaces and different speed values).
- The MSD controller $R_\epsilon(s)$ is implemented with a simpler PI control architecture (notice that this is another additional advantage of MSD control)

$$R_\epsilon(s) = K_\epsilon \frac{(1 + \tau_\epsilon s)}{s},$$

and with $\alpha = 0.9$. Also the MSD controller has been tuned to work satisfactorily in every working condition.

The results presented in the following refer to a front wheel.

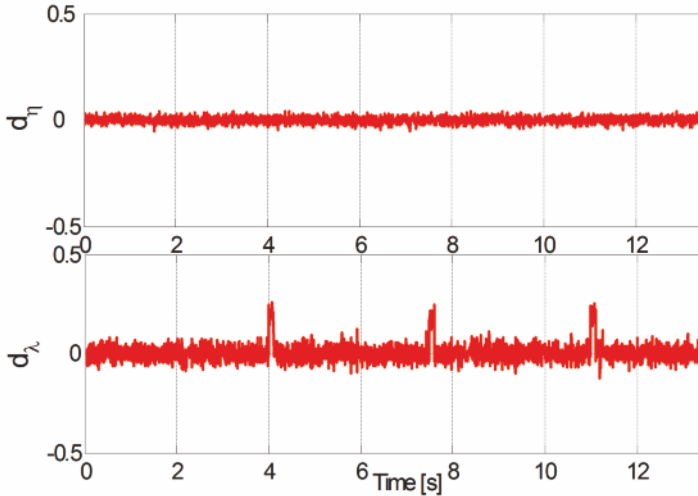


Figure 6.8 An example of measurement noises on λ and η used in the simulator

The first simulations have the goal of comparing the noise attenuation properties of the two control algorithms. In Figure 6.8 the measurement noises affecting the wheel deceleration and the wheel slip measurement are displayed. Notice that the variance of d_η is smaller than the variance of d_λ . Moreover, notice the different behaviour of the two measurement noises: d_η is essentially a broad-band stationary signal, while d_λ is characterised by huge spikes, due to poor speed estimation. Unfortunately, these spikes can hardly be reduced and they occur during hard braking, which is the typical working condition of active braking controllers.

In Figure 6.9 the time histories of the wheel slip during a hard braking manoeuvre on dry asphalt are displayed and MSD and slip control are compared. Notice that, as expected, the noise sensitivity of MSD control is remarkably lower than that of slip control; this results in a much smaller variation range of the actual wheel slip. Moreover, notice that MSD control has slightly better phase margin properties at low speed; as a matter of fact, the typical unstable behaviour that occurs at the end of the braking manoeuvre, *i.e.*, when the vehicle speed is very low (see the time interval $t \in [12, 14]$ s in Figure 6.9), arises later in MSD control. This result fully confirms the theoretical analysis performed in the simplified setting.

Finally, in Figures 6.10 and 6.11 the time histories of the wheel slip obtained with the MSD controller during a hard braking manoeuvre (in a noise-free setting) is shown, when a sudden change in the road surface occurs (from dry asphalt to snow in Figure 6.10, and from snow to dry asphalt in Figure 6.11). Very similar results can be obtained with the slip controller. Notice the remarkable robustness of the fixed-structure MSD controller; also notice that according to the MSD control rationale, the steady-state value of

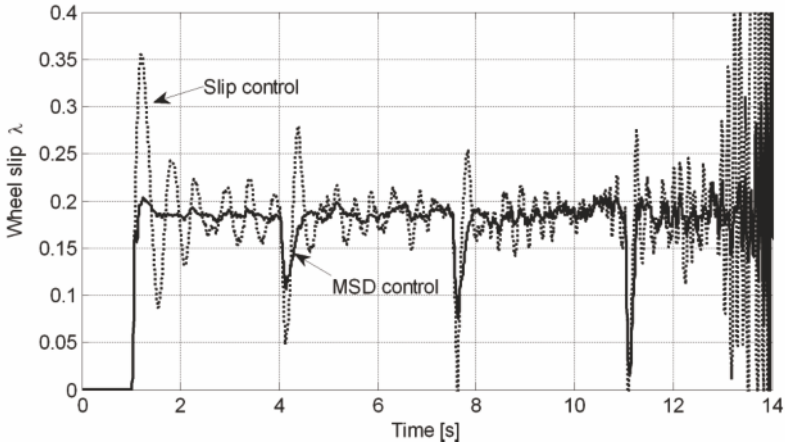


Figure 6.9 Time history of the wheel slip during a hard-braking manoeuvre on dry asphalt

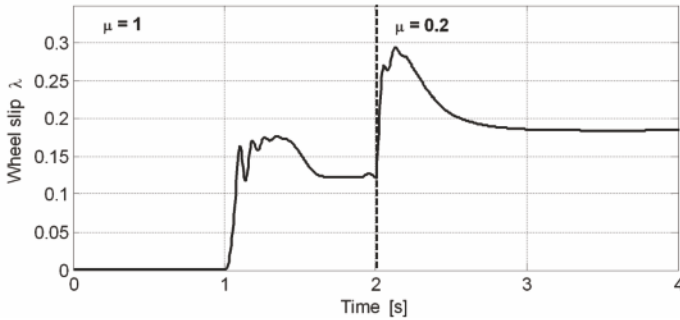


Figure 6.10 MSD control performance in a hard braking manoeuvre, with a sudden road-surface change from high to low grip road

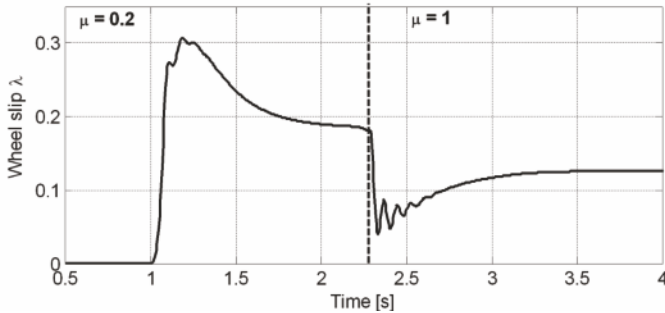


Figure 6.11 MSD control performance in a hard braking manoeuvre, with a sudden road-surface change from low to high grip road

the wheel slip changes when the friction curve changes according to different road surfaces (see Figure 6.2, which clearly shows this fact).

6.6 Summary

This chapter presented a wheel slip control strategy based on the idea of designing a standard SISO regulation loop on an output variable constituted by the convex combination of wheel slip and wheel deceleration. This control approach was referred to as MSD control.

The starting point of the MSD approach is to be found in [41, 69], where braking controllers based on modern electro-mechanical brakes are described, and which can be regarded as the state-of-the art in slip-controlled braking systems. The MSD approach was conceived to move one step further, so as to improve the performance of slip control by mixing slip and deceleration measurements.

Using a simple proportional-control regulation scheme this control structure was deeply analysed. Interestingly enough, MSD control inherently embodies, as extremal cases, also the more classical slip control and deceleration control schemes. Hence MSD control can move seamlessly between deceleration control and slip control. This is very appealing in sophisticated BBW systems, which may require a time-varying setting: emphasis on deceleration control during soft braking and emphasis on slip control in anti-lock conditions.

It has been shown that MSD control inherits all the appealing characteristics of slip control (unique equilibrium, fixed set-point, guaranteed closed-loop stability with a fixed structure linear time-invariant controller), but it overcomes the major flaw of slip control: its sensitivity to slip measurement errors.